water

MDPI

Article

Numerical Simulation of Hydro-Sedimentary Dynamics and Tidal Prism Responses to Reclamation Removal in Northern Liaodong Bay

Kun Wang [1,2], Chaokui Hu [1,2], Jinhao Wu [1,2], Zhaohui Wang [1,2], Guangjun Song [1,2], Yanjun Gong [1,2], Nan Li [1,2,*] and Lun Song [1,2,*]

[1] Liaoning Ocean and Fisheries Science Research Institute, Dalian 116023, China
[2] Key Laboratory of Protection and Utilization of Aquatic Germplasm Resource, Ministry of Agriculture and Rural Affairs, Dalian 116023, China
* Correspondence: linan_lab@163.com (N.L.); lsong2020@yeah.net (L.S.)

Abstract

Coastal reclamation projects have drastically altered hydrodynamic conditions, sediment transport, and tidal exchange in semi-enclosed bays. However, quantitative research on the ecological restoration effects achieved through reclamation removal remains limited for high-latitude cold coastal bays, such as the northern Liaodong Bay. In this study, a well-calibrated two-dimensional depth-averaged hydrodynamic–sediment fully coupled numerical model was developed based on the finite-volume method, employing an unstructured triangular mesh for flexible discretization and local refinement of complex coastal boundaries. The Smagorinsky subgrid-scale turbulence parameterization scheme was incorporated to close the momentum equations, and a multi-component sediment transport module was coupled with a multi-layer bed erosion–deposition module to achieve two-way feedback between hydrodynamic and sediment processes. Four restoration test scenarios were designed, including the baseline status, full reclamation removal, partial reclamation removal, and full removal combined with tidal creek dredging, to quantitatively analyze the spatiotemporal responses of flow field, suspended-sediment concentration, bed topography evolution, and tidal prism. A total of five numerical simulations were conducted: one for model validation (covering water level, current velocity, and suspended-sediment data) and four for simulating the four restoration test scenarios. The results show that reclamation removal hardly changes the overall tidal flow structure and spatial distribution of suspended sediment in the bay. Variations in flow and sediment are confined to a narrow zone within 500 m around the project area, exerting negligible impacts on the entire Liaodong Bay and the Liaohe Estuary. Natural tidal creek networks, as vital geomorphic units, can buffer large-scale hydrodynamic disturbances. After full reclamation removal, the average tidal prism of the bay increased from 2.76×10^7 m^3 under the baseline condition to 2.79×10^7 m^3 (a 1.27% increase); under the combined scheme of full removal and tidal creek dredging, it further increased to 2.82×10^7 m^3 (a 2.17% increase). This improvement is more pronounced during spring tides. This study confirms that reclamation removal avoiding major tidal creeks is a low-disturbance ecological restoration approach suitable for semi-enclosed estuarine bays in northern China. A combined restoration scheme of full removal and tidal creek dredging is recommended to enhance tidal connectivity. These findings can provide quantitative references for coastal reclamation management and tidal-flat ecological restoration in temperate semi-enclosed bays.

Check for updates

Academic Editor: Muhammad Hameed

Received: 28 September 2026
Revised: 28 October 2026
Accepted: 4 November 2026
Published: 7 November 2026

Copyright: © 2026 by the authors. Licensee MDPI, Basel, Switzerland. This article is an open access article distributed under the terms and conditions of the Creative Commons Attribution (CC BY) license.

Keywords: Liaodong Bay; reclamation removal; depth-averaged coupled hydrodynamic–sediment numerical model; tidal prism; ecological restoration

1. Introduction

Coastal land reclamation has been widely implemented across the globe to address land scarcity brought about by coastal urbanization and industrial development. Artificial land expansion effectively supports port construction, industrial layout and urban expansion, and greatly improves the carrying capacity of coastal regions for social and economic development. However, large-scale and intensive reclamation activities have profoundly transformed natural coastal geomorphology and hydro-sedimentary environments. Excessive artificial modification of shorelines breaks the original hydro-sedimentary equilibrium, reduces the effective water area of bays and weakens tidal exchange capacity. These changes further trigger persistent coastal siltation, tidal-flat shrinkage, habitat fragmentation and a series of ecological problems. Numerous semi-enclosed bays worldwide have suffered from degradation of tidal-flat wetland ecosystems and a decline in ecosystem services due to unregulated reclamation, posing severe threats to coastal ecological security [1–12].

Faced with ongoing ecological degradation caused by reclamation, coastal governance worldwide has gradually shifted to an ecology-oriented development mode over recent decades. Reclamation demolition and passive tidal-flat restoration have become mainstream remediation strategies to relieve ecological pressure and restore the functions of coastal wetlands. International experiences demonstrate the effectiveness of such approaches: Palacios et al. [13] documented successful tidal-flat restoration through managed realignment in the UK; Slinger et al. [14] reported on nature-based coastal solutions for reclamation removal in the Netherlands; Kiesel et al. [15] demonstrated marsh restoration outcomes following levee removal in California; Türker et al. [16] analyzed coastal reclamation removal impacts on hydrodynamics in Turkey; and Petti et al. [17] evaluated ecological recovery following reclamation removal in the Mediterranean. Removing unreasonable reclamation structures and restoring natural shorelines and tidal flats can gradually rehabilitate damaged hydrodynamic regimes and sediment transport processes. It also creates favorable conditions for the recovery of tidal-flat vegetation, reproduction of benthic organisms and inhabitation of waterbirds, and thus promotes the healthy succession of coastal ecosystems.

The northern Liaodong Bay is a typical semi-enclosed cold-water bay in the Bohai Sea. Located in the temperate monsoon zone, it features low water temperature and seasonal sea ice, representing a typical high-latitude cold coastal environment. The study area boasts extensive tidal-flat resources and well-developed dendritic tidal creek systems. As core corridors for material and energy exchanges between tidal flats and open waters, tidal creeks play an irreplaceable role in maintaining hydro-sedimentary balance and wetland ecological functions. In addition, the hydro-sedimentary evolution in this bay is highly sensitive to human interventions. Shoreline reconstruction and reclamation projects can directly alter tidal flow paths, sediment transport patterns and seabed erosion–deposition characteristics, thereby threatening the overall ecological stability of the bay.

Numerical simulation studies on Liaodong Bay have been continuously enriched in recent years. Most existing studies have focused on the adverse environmental impacts of historical reclamation projects, revealing their negative effects on flow fields, suspended-sediment distribution, seabed evolution, and the ecological environment [18–29]. Two-dimensional numerical modeling in Liaodong Bay has gradually evolved from early plane two-dimensional hydrodynamic models based on structured grids and finite-difference methods to depth-averaged hydrodynamic–sediment coupled models employing unstruc-

tured triangular meshes and the finite-volume method. Unstructured meshes can more flexibly fit complex boundaries such as coastlines, tidal flats, and tidal creek networks, and support local refinement in engineering areas and tidal creek zones. The finite-volume method facilitates the preservation of mass conservation and flux continuity under complex geometric boundaries. For turbulence closure, the Smagorinsky subgrid-scale parameterization scheme has been widely used to represent horizontal eddy viscosity [30–32], thereby improving the characterization of flow shear and subgrid-scale turbulent mixing. Meanwhile, the introduction of multi-component sediment transport modules and multi-layer bed erosion–deposition modules has enabled two-way feedback between hydrodynamic fields and bed erosion–deposition processes over tidal cycles. These achievements have laid a foundation for understanding the environmental costs of coastal reclamation, and the methodological advances have provided a reliable technical basis for quantitatively assessing hydro-sedimentary responses to reclamation and its subsequent removal. Nevertheless, specific research ideas concerning ecological restoration still need to be further enriched. First, few studies have conducted quantitative comparisons among multiple reclamation removal schemes, and the differences in hydro-sedimentary responses under different removal scales and restoration modes remain unclear. Second, the inherent buffering mechanism of natural tidal creek networks against hydrodynamic disturbances during restoration has not been systematically elucidated. Third, there is a lack of accurate quantification of how different removal schemes affect local hydrodynamics, sedimentary environments, and the bay-scale tidal prism, which hinders scientific decision-making for local tidal-flat ecological restoration.

To enrich the above research content, this study constructs a validated two-dimensional coupled hydro-sedimentary numerical model and establishes four comparative restoration scenarios. The main research objectives are as follows: (1) quantify the spatiotemporal variations in the flow field, suspended sediment and seabed erosion–deposition under different reclamation removal modes; (2) clarify the buffering and regulating mechanism of tidal creek systems in response to hydrodynamic changes; (3) evaluate the tidal prism enhancement efficiency of various restoration schemes under spring and neap tidal conditions; (4) propose the most suitable restoration strategy among the test scenarios for semi-enclosed estuarine bays in northern China. This work is expected to provide scientific support for reclamation regulation and the protection and ecological restoration of tidal-flat wetlands in temperate semi-enclosed bays.

2. Materials and Methods

2.1. Model and Governing Equations

A depth-integrated two-dimensional shallow-water hydrodynamic model coupled with a suspended-sediment transport module is employed in this study, consisting of a continuity equation, a momentum equation, a sediment transport equation and an empirical tidal prism calculation formula.

Continuity equation

$$\frac{\partial h}{\partial t} + \frac{\partial hu}{\partial x} + \frac{\partial hv}{\partial y} = hS \tag{1}$$

Momentum equations

$$\begin{aligned} &\frac{\partial hu}{\partial t} + \frac{\partial hu^2}{\partial x} + \frac{\partial hvu}{\partial y} = fvh - gh\frac{\partial \eta}{\partial x} - \frac{h}{\rho_0}\frac{\partial p_a}{\partial x} - \frac{gh^2}{2\rho_0}\frac{\partial \rho}{\partial x} + \frac{\tau_{sx}}{\rho_0} - \frac{\tau_{bx}}{\rho_0} \\ &-\frac{1}{\rho_0}\left[\frac{\partial s_{xx}}{\partial x} + \frac{\partial s_{xy}}{\partial y}\right] + \frac{\partial}{\partial x}(hT_{xx}) + \frac{\partial}{\partial y}\left(hT_{xy}\right) + hu_sS \end{aligned} \tag{2}$$

$$\begin{aligned} &\frac{\partial hv}{\partial t} + \frac{\partial hv^2}{\partial x} + \frac{\partial huv}{\partial y} = fuh - gh\frac{\partial \eta}{\partial y} - \frac{h}{\rho_0}\frac{\partial p_a}{\partial y} - \frac{gh^2}{2\rho_0}\frac{\partial \rho}{\partial y} + \frac{\tau_{sy}}{\rho_0} - \frac{\tau_{by}}{\rho_0} \\ &-\frac{1}{\rho_0}\left[\frac{\partial s_{yx}}{\partial x} + \frac{\partial s_{yy}}{\partial y}\right] + \frac{\partial}{\partial x}\left(hT_{yx}\right) + \frac{\partial}{\partial y}\left(hT_{yy}\right) + hv_sS \end{aligned} \tag{3}$$

where t is the time coordinate; x and y are spatial coordinates (m); u and v are the depth-averaged horizontal velocity components (m/s); η is water level (m); $h = \eta + d$ is total water depth (m); d is still-water depth (m); ρ is water density (kg/m^3); ρ_0 is relative density; S is a source–sink term; p_a is atmospheric pressure (Pa); u_s and v_s are the velocities of source–sink terms (m/s); $f = 2\omega\sin\varphi$, where ω is the Earth's angular velocity of rotation and φ is geographic latitude; (τ_{sx},τ_{bx}), (τ_{sy},τ_{by}) are the surface wind and bed shear stress components in the x and y directions; and T_{xx}, T_{xy}, T_{yx}, T_{yy} are horizontal stresses (Pa), including viscous stress, turbulent friction and advective friction.

Sediment transport equation

$$\frac{\partial C}{\partial t} + u\frac{\partial C}{\partial x} + v\frac{\partial C}{\partial y} = \frac{1}{h}\frac{\partial}{\partial x}(hD_x\frac{\partial C}{\partial x}) + \frac{1}{h}\frac{\partial}{\partial y}(hD_y\frac{\partial C}{\partial y}) + Q_L C_L\frac{1}{h} - S_{cq} \quad (4)$$

where c is the mass-averaged concentration of sediment in the water column (kg/m^3); D_x and D_y are diffusion coefficients (m^2/s); S_{cq} is the sediment deposition–erosion term; Q_L is the sediment source flux per unit horizontal area (m^3·s^{-1}); and C_L is the sediment source concentration (kg/m^3).

Calculation formula of bay tidal prism

$$P = \overline{\eta} \cdot \overline{A} \quad (5)$$

where P is the tidal prism (m^3); $\overline{\eta}$ is the mean tidal range (m); and $\overline{A}$ is the mean water area (m^2).

2.2. Model Setup

2.2.1. Computational Domain

The computational domain covers the northern part of Liaodong Bay, bounded by control points A (120°31.2′ E, 40°13.2′ N) and B (121°25.8′ E, 39°45.0′ N). An unstructured triangular mesh is adopted to flexibly fit the coastline, with local mesh refinement implemented in the reclamation project area to improve topographic adaptability and computational precision. A mesh sensitivity analysis was conducted by comparing three mesh configurations: a coarse mesh (38,521 nodes/75,203 elements), a medium mesh (62,195 nodes/121,019 elements), and a fine mesh (95,847 nodes/186,432 elements). The medium mesh was selected as the final computational mesh because it achieves a balance between computational efficiency and simulation accuracy. Compared with the fine mesh, the medium mesh yields tidal level validation errors of less than 0.10 m and flow velocity errors of less than 8%, while significantly improving computational efficiency. The entire computational domain contains 62,195 nodes and 121,019 triangular elements, with a minimum mesh size of 10 m near the engineering zone. The coordinates of the boundary-control points of the computational domain are detailed in Table 1. The bathymetry and mesh layout before and after the reclamation removal restoration activities are shown in Figures 1–3. Specifically, Figure 1 presents the computational domain mesh and bathymetric distribution; Figure 2 compares the local mesh before and after the restoration activities; and Figure 3 illustrates the local bathymetry before and after the restoration activities. The rectangular box indicates the extent of the key study area.

Table 1. Coordinates of boundary points in the computational domain.

Point Number	Longitude (E)	Latitude (N)
A	120°31.2′	40°13.2′
B	121°25.8′	39°45.0′

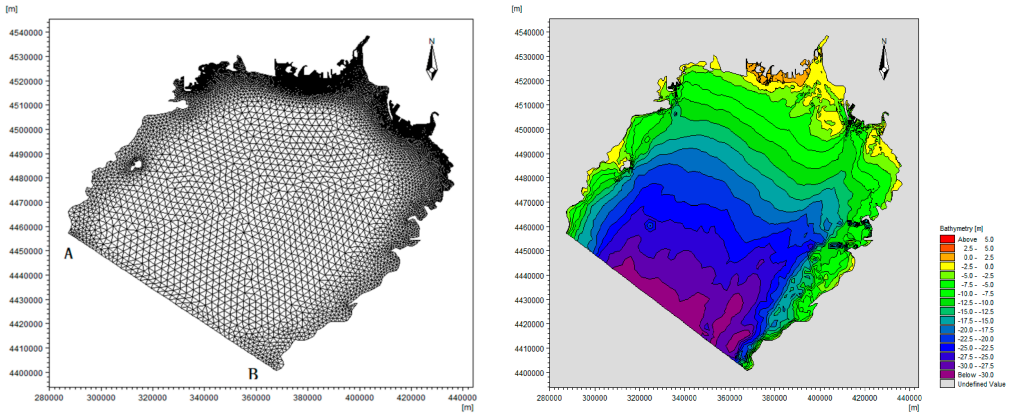


Figure 1. Computational domain, mesh and bathymetry distribution.

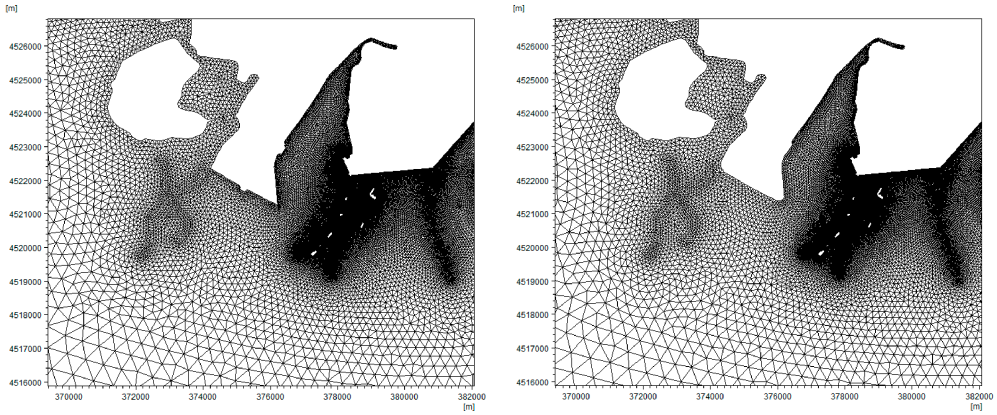


Figure 2. Local mesh before and after the restoration activities.

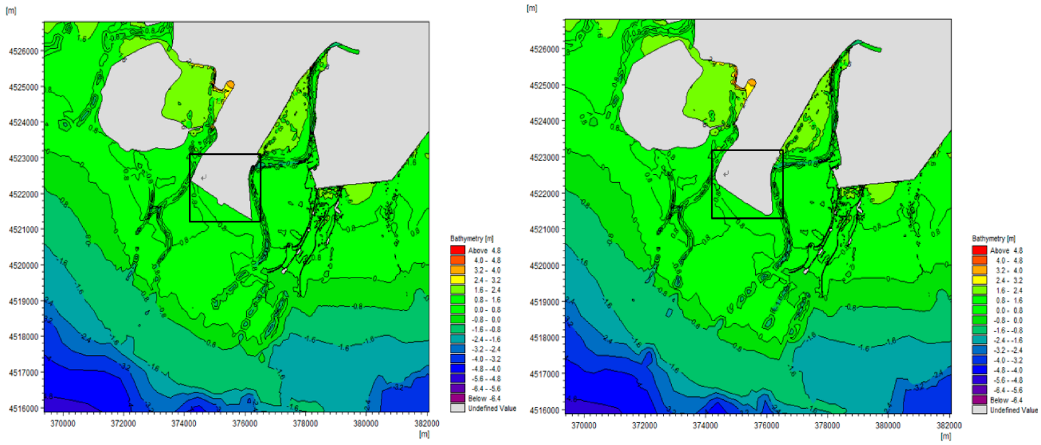


Figure 3. Local water depth maps before and after the restoration activities.

2.2.2. Model Solution Conditions and Parameter Settings

In this study, a zero normal velocity condition is applied at closed land boundaries. A dynamic wetting and drying algorithm is adopted for intertidal flat boundaries to simulate the periodic inundation and exposure of tidal flats caused by tidal fluctuations [33,34]. Time-varying water level series obtained from tidal harmonic analysis are imposed on the lateral open boundaries. All hydrodynamic and sediment variables across the entire computational domain are initialized using cold start (i.e., initial velocity and water level perturbations set to zero). Horizontal eddy viscosity is calculated by the classic Smagorinsky

subgrid model [30–32], and the initial suspended-sediment concentration field is set based on Dou Guoren's empirical sediment carrying capacity formula [35]. The densities of water and sediment are set to 1000 kg/m^3 and 2650 kg/m^3, respectively.

The bottom shear stress is derived based on the Nikuradse roughness coefficient and the depth-averaged flow velocity. For sandy coasts, the roughness is taken as 2.5 times the median grain size, whereas for muddy coasts, in addition to grain resistance, bedform resistance is also considered, typically with a value of 0.001 m.

In the present model, bed sediment is classified into three components: sand (0.063–2 mm), coarse silt (0.03–0.063 mm), and fine-grained sediment (<0.03 mm) that undergoes flocculation upon entering the water column. Since the sediment dynamic properties of the bed vary vertically with depth, the bed is stratified, with specific sediment parameters assigned to each layer. Erosion initiates from the surface layer; calculations for the underlying layer commence only after the top layer has been completely eroded. Based on historical experience and the specific seabed conditions of the study area, the thickness of the topmost layer is set to 0 m (initially serving only for deposition), while the second layer is set to 1 m.

Regarding settling velocities, for fine-grained sediment smaller than 0.03 mm, the flocculation settling velocity typically ranges between 0.1 and 0.6 mm/s; a midpoint value of 0.3 mm/s is adopted in this model. For sediment larger than 0.03 mm, flocculation effects are neglected, and the settling velocity is calculated using the Zhang Ruijin formula, with empirical coefficients of 1.22 and 4.27. Consequently, the settling velocities for the three sediment components are determined to be 0.8 mm/s, 0.3 mm/s, and 0.1 mm/s, respectively. The critical erosion shear stress for bed sediment generally ranges from 0.05 to 0.1 N/m^2; through model calibration, values of 0.07 N/m^2, 0.05 N/m^2, and 0.01 N/m^2 are applied in this numerical model. The erosion rate, which depends on the physicochemical properties of the bed, is set to 1.0×10^{-6} kg/m^2/s in the simulation. Specifically, for the first bed layer (semi-consolidated layer), the critical erosion shear stress is 0.15 N/m^2, while for the second layer (hard mud layer), it is 0.25 N/m^2.

The hydrodynamic forces influencing sediment transport in the study area are primarily waves and tides; therefore, both wave and sediment effects must be simultaneously considered in the sediment model. Under fair weather conditions, waves are relatively small; however, during typhoons or southeasterly/southerly wind events, waves become larger. Under wave action, sediment moves laterally, with coarse particles migrating shoreward and fine particles dispersing seaward, forming a well-sorted sandy beach. Over recent years, the sub-marine topography near the study area has remained stable. Currently, to investigate the impact of restoration activities on sediment transport, waves are incorporated as a calibration parameter. The present reclamation area is located at the bottom of Liaodong Bay, which opens to the south. Waves in this region are predominantly from the SW–SE directions, with the prevailing wave direction at the bottom of Liaodong Bay and its adjacent waters being from the south (S) and the secondary prevailing direction being from the west-southwest (WSW). The annual average wave height in this area typically ranges from 0.5 to 1.5 m. Therefore, in the model, a wave with a predominant direction biased toward the south is selected as the representative main wave direction, with a representative wave direction of S, a representative average wave height of 0.8 m, and a wave period of 5.0 s, which are incorporated into the model for simulation.

2.2.3. Scenario Design

Four mutually controlled scenarios with identical model parameters were established to isolate the individual and combined effects of reclamation removal and tidal creek dredging: S1 (baseline)—original reclamation completely retained as the control group;

S2 (full removal)—all artificial reclamation structures entirely demolished; S3 (partial removal)—only partial regional reclamation (artificial structures 6# and 6#E, representing approximately 50% of total reclaimed area based on spatial distribution analysis) removed (50% total demolition); S4 (composite restoration)—full reclamation removal + 10 m width expansion of the primary tidal creek channel. The selection of a 50% demolition ratio in S3 is based on the spatial feasibility assessment: structures 6# and 6#E are located in the peripheral zone of the reclamation area and are hydraulically isolated from the main tidal flow path, making their removal a conservative test of partial restoration efficacy. Structures 6# and 6#E are located in the peripheral zone of the reclamation area and are hydraulically isolated from the main tidal flow path, making their removal a conservative test of partial restoration efficacy. The 10 m widening in S4 was determined through preliminary hydraulic calculations to ensure the tidal creek cross-section could accommodate the increased tidal prism without inducing excessive scouring of the creek bed, based on the empirical relationship between channel width and discharge capacity in similar semi-enclosed bays.

2.3. Model Validation

2.3.1. Data Collection

This study used recent synchronous hydrological and sediment field data collected at six nearshore monitoring stations in the study area for model calibration. The monitoring network consisted of two tidal stations, two current stations and two suspended-sediment stations. The datasets included continuous time-series observations of tidal level, flow velocity, flow direction and in situ suspended-sediment concentration. The coordinates of all stations are presented in Table 2 and Figure 4.

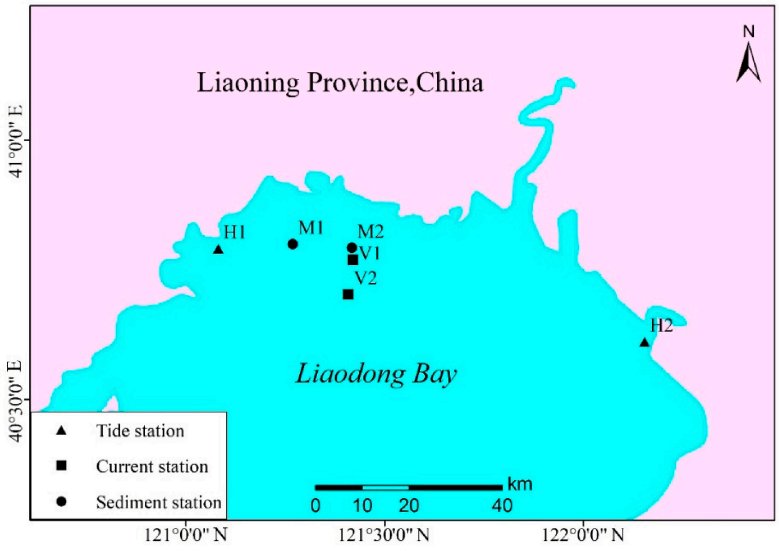


Figure 4. Sketch of hydrological and sediment observation stations.

Table 2. Locations of observation stations.

Number	Longitude (E)	Latitude (N)	Station ID	Type
1	121°04.0′	40°48.0′	H1	Tidal station
2	122°09.0′	40°38.0′	H2	Tidal station
3	121°24.5′	40°47.0′	V1	Current station
4	121°23.9′	40°43.0′	V2	Current station
5	121°15.3′	40°48.7′	M1	Sediment station
6	121°24.3′	40°48.4′	M2	Sediment station

2.3.2. Tidal Level Validation

The temporal variations in simulated and measured tidal levels at the two stations are plotted in Figure 5. The results indicate that the simulated tidal levels agree well with the measured data. The phase error between simulated and measured high and low waters is less than 0.5 h, and the amplitude error is less than 5 cm. Overall, the numerical model satisfactorily captures the propagation of flood and ebb tides, and the simulated results are highly consistent with field measurements.

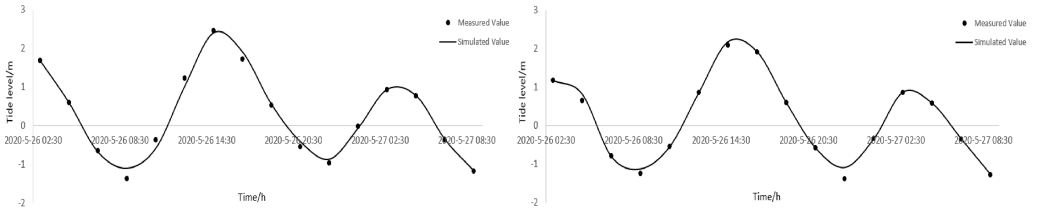


Figure 5. Comparison of tidal levels at H1 and H2.

2.3.3. Current Validation

The temporal variations in simulated and measured flow velocities at the two current observation stations are presented in Figures 6 and 7. The comparison shows good agreement between simulated and measured flow velocities, demonstrating that the numerical model can effectively reproduce the temporal evolution of currents in the study area. Combined with the aforementioned tidal level validation results, it is confirmed that the mesh, bathymetry, boundary conditions and parameters adopted in the model are accurate and reasonable. The model can provide a reliable hydrodynamic background field for subsequent numerical simulations of sediment transport and water exchange.

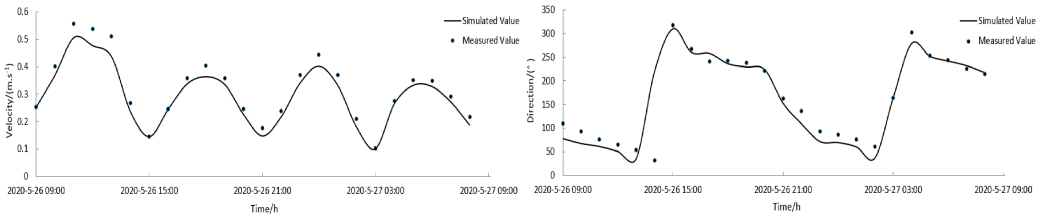


Figure 6. Comparison of velocity and direction at V1.

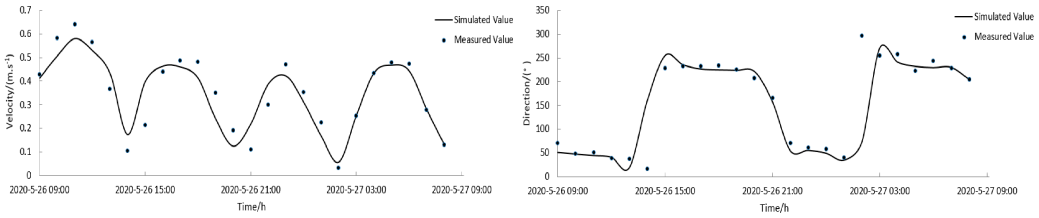


Figure 7. Comparison of velocity and direction at V2.

2.3.4. Suspended-Sediment Validation

To further verify the accuracy of the suspended-sediment model, the simulated suspended-sediment concentration (SSC) is compared with field measurements in Figure 8. The results show that the simulated SSC values are in good agreement with the in situ observations. The model fully meets the requirements for subsequent numerical simulation and prediction of seabed topography and geomorphology.

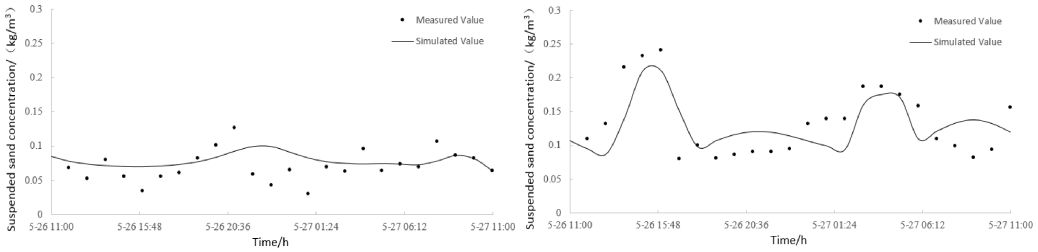


Figure 8. Comparison of suspended-sediment concentration at M1 and M2.

3. Parameter Sensitivity Analysis and Uncertainty Discussion

3.1. Parameter Sensitivity Analysis

A relative sensitivity index is adopted to quantify the sensitivity of key model parameters:

$$S = \frac{|E_2 - E_1|}{E_1} \times 100\% \quad (6)$$

where S is parameter sensitivity; E1 is the simulation error under the baseline parameter setup; and E2 is the simulation error after ±20% parameter perturbation. Three dominant parameters, bed roughness coefficient n, the Smagorinsky eddy viscosity coefficient Cs and critical bed shear stress for sediment initiation τ_c, are individually perturbed within ±20% to conduct single-factor sensitivity tests.

Bed roughness n: When n increases by 20%, the flow velocity error rises from 3.12% to 9.35%, with S = 6.23%; when n decreases by 20%, the velocity error reduces to 2.01% with S = 3.56%. Bed roughness presents high sensitivity to nearshore hydrodynamic calculation.

Smagorinsky coefficient Cs: The overall variation in flow error is less than 3.5% under ±20% adjustment.

Critical shear stress τ_c: This parameter only affects suspended-sediment distribution with a maximum sediment error variation of S = 5.72%, while tidal level and flow field remain nearly unchanged.

The final parameter configuration adopted in this study was determined based on the above sensitivity test results, and all selected parameter values fall within physically reasonable ranges.

3.2. Model Uncertainty Assessment

The mean relative error is calculated to quantitatively evaluate overall model uncertainty:

$$\bar{\varepsilon} = \frac{1}{N}\sum_{i=1}^{N}\frac{|S_{sim,i} - S_{obs,i}|}{S_{obs,i}} \times 100\% \quad (7)$$

where $\bar{\varepsilon}$ is the mean relative error; $S_{sim,I}$ is the simulated value; $S_{obs,I}$ is the observed value; and N is the total sample number. The calculated average relative error is 7.82% for tidal elevation, 8.95% for flow velocity and 25.71% for suspended-sediment concentration.

Three primary uncertainty sources are summarized as follows:

(1) Topographic data: Fixed static bathymetry ignores seasonal bed erosion–deposition variation, resulting a systematic error of approximately 2–4%.
(2) Open boundary condition: Tidal boundaries are derived from harmonic analysis without incorporating episodic storm surge and short-term wind forcing, which may magnify the model bias under extreme meteorological conditions.
(3) Simplification of sediment module: Wind–wave resuspension and sea-ice effects are excluded from the current model, leading to minor bias in the prediction of long-term morphological evolution prediction.

Under normal astronomical tidal conditions, the overall simulation error is acceptable for inter-comparison among the four restoration scenarios, and the core quantitative conclusions of different restoration scenarios are not affected by existing uncertainties.

4. Results and Discussion

4.1. Basin-Scale and Local Hydrodynamic Spatial Responses

The results of hydrodynamic numerical simulation predictions indicate that under the baseline condition, flood tide propagates from southwest to northeast with a maximum nearshore velocity of 1.0 m/s, while ebb tide flows reversely (NE-SW) with a peak velocity of ~0.8 m/s. All restoration schemes fail to alter the large-scale circulation structure of Northern Liaodong Bay; hydrodynamic modifications are geographically restricted to the vicinity of demolished reclamation. Among the four scenarios, S4 generates the most prominent local flow acceleration (12.3% velocity increment) due to the enlarged tidal creek cross-section and enhanced tidal conveyance capacity. Figure 9 illustrates the location of the restoration project and depicts the shoreline changes. Here, P1 and P2 represent the boundary points of the study area between the reclamation dikes, which also serve as the reference points for the subsequent tidal prism calculation. Figures 10 and 11 present the distributions of the planar flow fields under different scenarios and tidal conditions.

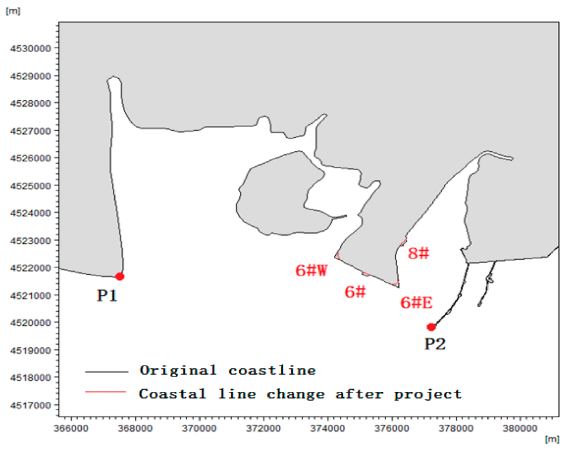


Figure 9. Project location and shoreline changes.

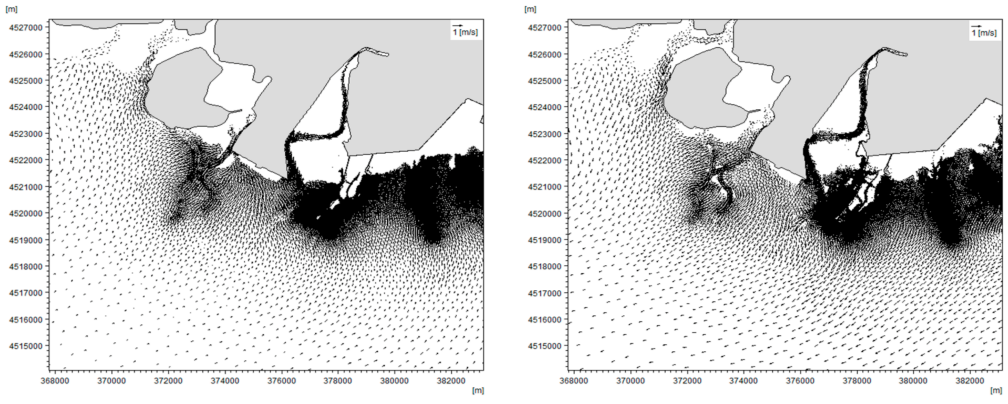


Figure 10. Local flow field at flood peak and ebb peak under the existing condition.

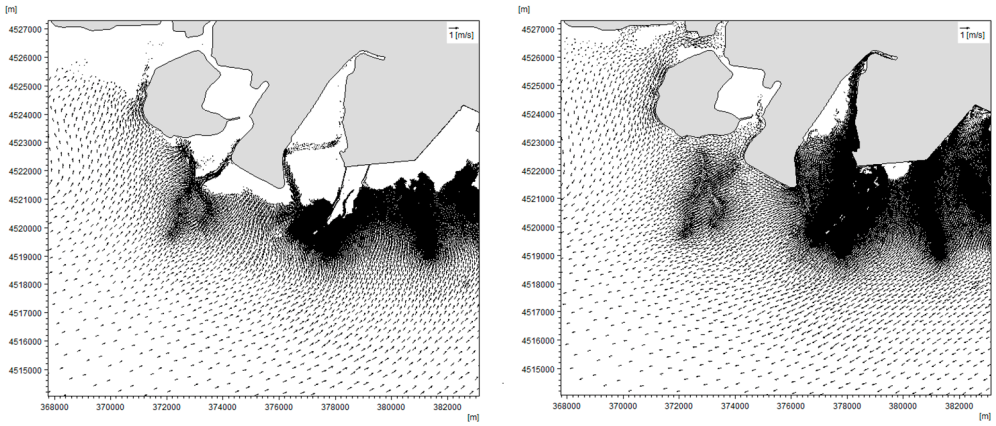


Figure 11. Local flow field at flood peak and ebb peak after the restoration activities.

4.2. Quantitative Statistical Analysis of Hydrodynamic Variation at Gradient Distances

A total of 24 sampling points were arranged at three gradient distances (500 m, 1500 m, and 3000 m from the project area) to quantitatively characterize the spatial pattern of hydrodynamic disturbances. The locations of the sampling points are shown in Figure 12, and the statistical results are presented in Tables 3 and 4 as follows:

(1) Within the 500 m zone adjacent to the reclamation, the flow velocity changes vary distinctly across scenarios, with S4 presenting the maximum flow increment, followed by S2 and S3.

(2) At distances beyond 1500 m from the restoration area, the relative velocity fluctuation generally falls below 10%, and the impacts are negligible at 3000 m offshore.

(3) The disturbance intensity follows the ranking S4 > S2 > S3 > S1, demonstrating that tidal creek dredging can effectively amplify the hydrodynamic improvement effect of reclamation removal.

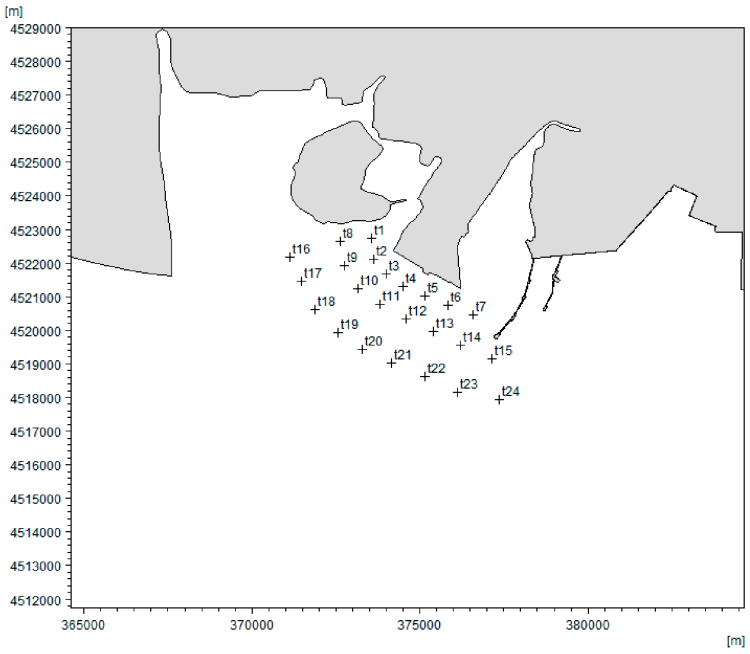


Figure 12. Locations of comparison points.

Table 3. Variation in velocity at maximum flood.

No.	Distance (m)	Velocity Before Demolition (cm/s)	Velocity After Demolition (cm/s)	Velocity Difference (cm/s)	Percentage	Direction Before Demolition (°)	Direction After Demolition (°)	Direction Difference (°)
t1	500	24.5	30.6	6.1	24.83%	72.5	46.8	25.8
t2	500	21.5	23.7	2.2	10.44%	62.8	36.3	26.4
t3	500	21.4	22.2	0.8	3.51%	41.9	70.8	−28.9
t4	500	23.6	21.9	−1.7	−7.13%	350.3	352.4	−2.1
t5	500	23.8	28.1	4.3	18.19%	347.4	358.8	−11.4
t6	500	20.7	27.5	6.8	33.11%	1.5	17.1	−15.6
t7	500	53.2	55.0	1.8	3.34%	2.9	2.9	0.0
t8	1500	15.2	16.9	1.7	10.90%	69.9	69.8	0.1
t9	1500	27.4	25.6	−1.8	−6.67%	66.9	51.7	15.2
t10	1500	36.7	33.4	−3.3	−9.09%	8.7	1.6	7.1
t11	1500	30.2	28.4	−1.8	−5.92%	29.3	19.9	9.4
t12	1500	35.7	35.7	0.0	0.05%	22.5	16.1	6.4
t13	1500	36.1	39.4	3.3	9.13%	356.1	357.6	−1.5
t14	1500	35.7	33.0	−2.8	−7.74%	339.5	340.5	−1.0
t15	1500	30.4	33.2	2.8	9.18%	324.5	322.9	1.6
t16	3000	25.6	26.0	0.4	1.67%	29.6	16.7	12.8
t17	3000	23.8	25.4	1.6	6.57%	26.9	18.0	8.8
t18	3000	23.8	25.5	1.7	7.10%	25.7	16.4	9.4
t19	3000	23.9	24.0	0.1	0.46%	36.4	18.6	17.8
t20	3000	26.6	26.3	−0.2	−0.89%	35.3	20.8	14.5
t21	3000	25.4	23.0	−2.4	−9.26%	25.7	16.1	9.6
t22	3000	26.6	24.0	−2.6	−9.74%	4.3	3.1	1.2
t23	3000	23.8	24.1	0.3	1.14%	7.4	357.7	−350.3
t24	3000	18.5	17.2	−1.3	−6.96%	16.0	6.8	9.2

Table 4. Variation in velocity at maximum ebb.

No.	Distance (m)	Velocity Before Demolition (cm/s)	Velocity After Demolition (cm/s)	Velocity Difference (cm/s)	Percentage	Direction Before Demolition (°)	Direction After Demolition (°)	Direction Difference (°)
t1	500	13.7	17.1	3.4	24.86%	244.4	242.7	1.7
t2	500	20.0	18.0	−2.0	−10.02%	236.1	253.3	−17.2
t3	500	19.8	17.9	−1.8	−9.34%	202.9	260.3	−57.4
t4	500	15.7	16.4	0.7	4.60%	165.5	261.6	−96.1
t5	500	20.2	17.2	−3.1	15.16%	169.1	264.1	−95.0
t6	500	27.6	24.8	−2.7	−9.89%	198.6	249.4	−50.8
t7	500	28.8	30.8	2.0	6.78%	183.5	196.0	−12.5
t8	1500	11.0	12.0	1.0	9.11%	252.5	269.8	−17.3
t9	1500	26.0	23.4	−2.6	−10.04%	232.4	244.0	−11.6
t10	1500	31.7	32.9	1.2	3.83%	167.3	208.2	−40.9
t11	1500	26.2	26.4	0.2	0.70%	189.2	237.9	−48.7
t12	1500	30.1	27.2	−2.9	−9.60%	205.5	238.9	−33.4
t13	1500	30.9	28.5	−2.4	−7.87%	191.7	232.7	−41.1
t14	1500	29.8	27.6	−2.1	−7.19%	182.3	237.2	−55.0
t15	1500	35.2	27.1	−8.1	−22.99%	161.2	215.1	−54.0
t16	3000	26.1	24.0	−2.0	−7.72%	213.6	216.1	−2.5
t17	3000	26.4	25.7	−0.7	−2.53%	215.4	225.2	−9.8
t18	3000	26.4	24.1	−2.3	−8.64%	222.7	233.1	−10.4
t19	3000	27.9	28.4	0.5	1.78%	235.5	243.8	−8.3
t20	3000	37.7	36.7	−1.0	−2.67%	221.9	242.3	−20.4
t21	3000	33.6	32.3	−1.3	−3.86%	216.5	236.1	−19.6
t22	3000	41.4	43.9	2.5	6.08%	188.6	225.5	−36.9
t23	3000	39.2	35.4	−3.9	−9.84%	194.5	220.6	−26.0
t24	3000	37.2	38.3	1.1	2.83%	210.7	225.8	−15.0

4.3. Spatial Distribution Characteristics of Suspended Sediment

The variations in suspended-sediment concentration (SSC) under different engineering scenarios are presented in Figures 13–15.

(1) Baseline scenario and overall pattern (Figures 13 and 14): In baseline Scenario 1 (Figure 13) and in Scenarios 2 and 4 (Figure 14), distinct high-concentration cores

(>0.6 kg/m^3) are mainly distributed along the shallow intertidal flats and near the tidal creek mouths. This pattern is primarily driven by periodic tidal resuspension and friction-induced energy dissipation. In contrast, the offshore deep-water region maintains a low background SSC of 0.1–0.2 kg/m^3.

(2) Impact of the widened tidal creek (Scenario 4): A comparison between Scenario 1 (Figure 13) and Scenario 4 (right panel of Figure 14) shows that the maximum SSC near the tidal creek mouth decreases. In Scenario 1, the peak SSC exceeds 1.36 kg/m^3, whereas in Scenario 4 it falls within the range of 1.12–1.34 kg/m^3. This indicates that widening the tidal creek enhances tidal flushing capacity, thereby promoting sediment dispersion and slightly reducing the peak nearshore SSC.

(3) Difference maps (Figure 15): Figure 15 further quantifies these changes. The difference maps show that the SSC changes induced by the various scenarios are relatively small, mostly within ±0.1 kg/m^3. This confirms that the demolition and restoration activities do not alter the overall large-scale pattern of sediment distribution.

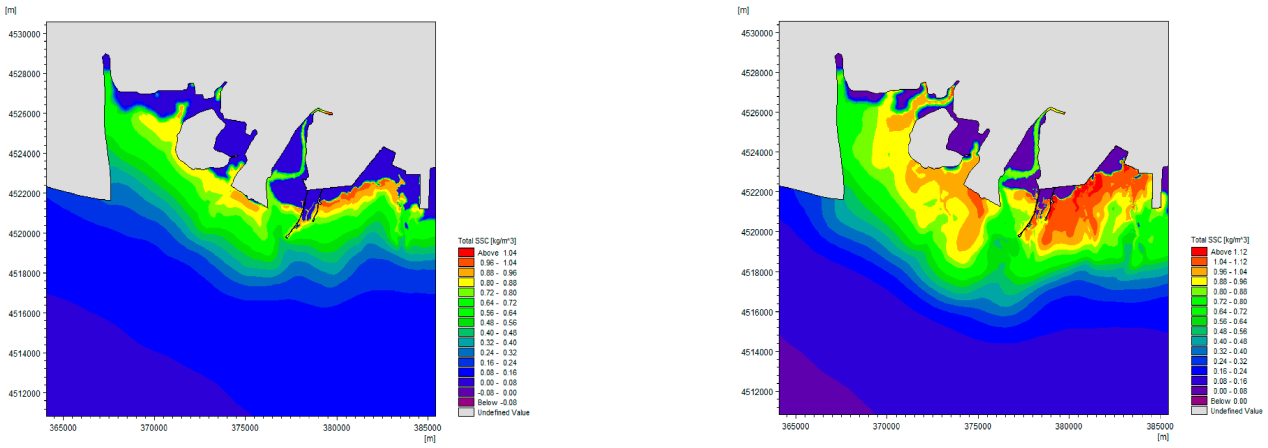


Figure 13. SSC distribution under Scenario 1.

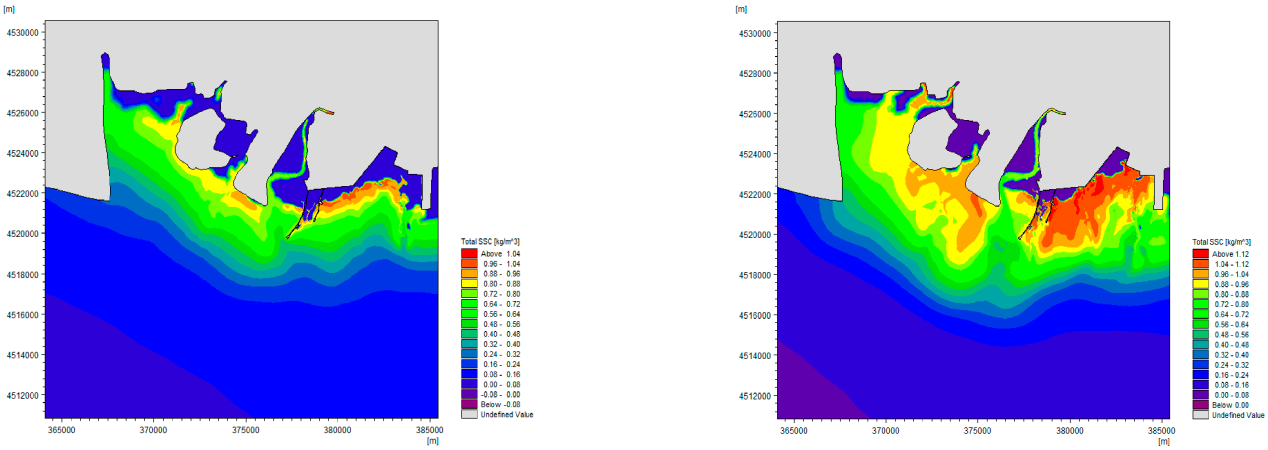


Figure 14. SSC distribution under Scenarios 2 and 4.

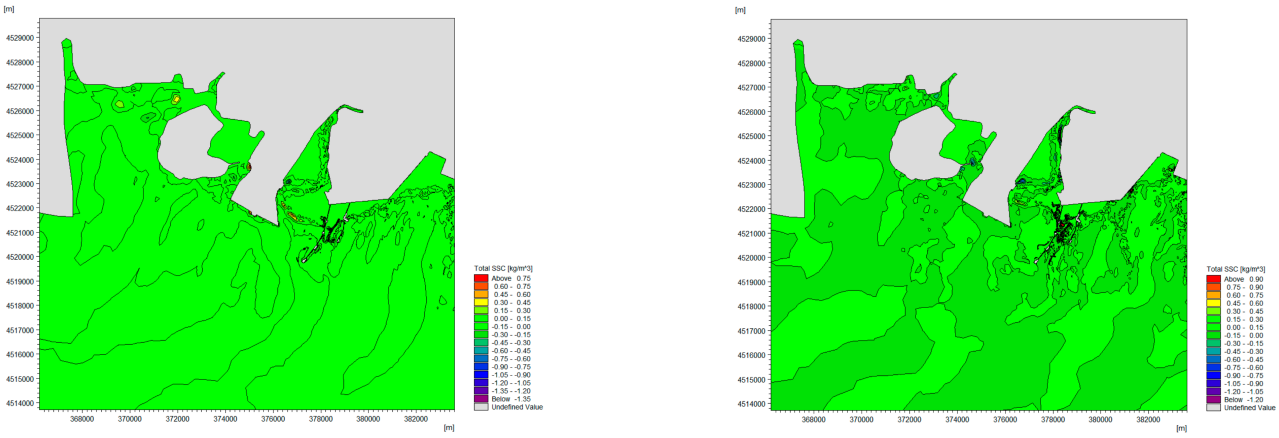


Figure 15. SSC difference maps.

4.4. Seabed Erosion–Deposition Evolution

The distributions of erosion and deposition before and after the restoration activities are illustrated in Figure 16. The composite restoration scheme (S4) successfully optimizes the nearshore bed morphology toward a more natural state. As shown in the figure, the study area is generally dominated by mild siltation (indicated by light orange and green zones, mostly 0.05–0.15 m) over the shallow intertidal flats, while slight offshore erosion (light blue zones) occurs in the deeper channels. Notably, the difference maps confirm that the annual bed elevation change remains within ±0.15 m across the entire bay under all scenarios, with no large-scale abnormal scour (deep blue zones) or excessive siltation (dark red zones) observed.

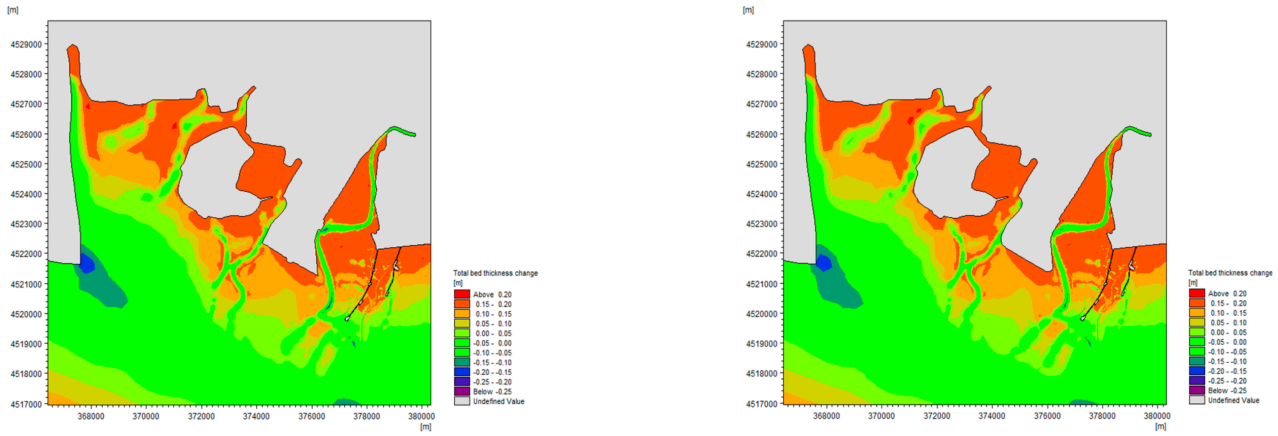


Figure 16. Erosion and deposition distribution before and after the restoration activities.

4.5. Quantified Tidal Prism Responses Under Different Restoration Scenarios

The bay water area and shoreline changes along the cross-section between P1 and P2 are summarized in Tables 5 and 6. Tidal prism is positively correlated with the extent of demolition range and tidal creek dredging. As shown in Table 7, the average tidal prism increases by 0.51% (S3), 1.27% (S2), 2.17% (S4) compared with the baseline S1. The spring tide shows significantly higher tidal prism growth amplitude than neap tide, owing to stronger tidal dynamic forcing.

Table 5. Variations in coastline and area in the bay area.

Working Condition	Coastline Length/km	Bay Mouth Width/km	Sea Area/km^2
Before demolition	4.23	9.8	54.18
After demolition	4.16	9.8	54.27

Table 6. Shoreline length and water area under four scenarios.

Scenario	Shoreline (km)	Bay Mouth (km)	Area (km^2)
S1	4.23	9.8	54.18
S2	4.16	9.8	54.27
S3	4.19	9.8	54.22
S4	4.12	9.8	54.33

Table 7. Tidal prism under four scenarios.

Scenario	Spring (10^7 m^3)	Neap (10^7 m^3)	Mean (10^7 m^3)	Increase (%)
S1	3.45	2.06	2.76	0
S2	3.50	2.08	2.79	1.27
S3	3.47	2.07	2.77	0.51
S4	3.55	2.09	2.82	2.17

4.6. Mechanism Discussion

4.6.1. Spatial Constraint Effect of Reclamation Removal Impact

Consistent with previous studies on Jiaozhou Bay and the Jiulong Estuary [2,5], our results show that reclamation removal in semi-enclosed bays triggers only localized hydro-sedimentary adjustment rather than basin-wide environmental change. The disturbance decays rapidly with offshore distance and becomes negligible beyond approximately 1500 m, which can be attributed to the large water storage capacity of Liaodong Bay buffering the relatively minor shoreline variation. This finding reinforces the view that semi-enclosed bays can absorb limited shoreline perturbations without fundamentally altering regional hydrodynamics [2,5].

4.6.2. Tidal Creek Inherent Buffering Mechanism

Beyond this spatial constraint, this study further identifies the natural tidal creek network as a dominant buffering mechanism controlling the intensity of environmental response during tidal-flat restoration. The branched creek system connects offshore open waters with inland tidal flats, dispersing flow changes induced by reclamation removal and preventing anomalous hydrodynamic signals from propagating into peripheral waters. Compared with previous restoration studies that have mainly emphasized the magnitude of shoreline change or the recovery of tidal area [2,5,10,27], this study highlights a process-based mechanism: the pre-existing tidal creek network regulates the redistribution of tidal prism and dampens hydrodynamic perturbations through its branching geometry and hydraulic connectivity.

This tidal creek buffering mechanism helps explain why moderate reclamation removal does not break regional hydro-sedimentary stability in northern Liaodong Bay, even when artificial structures are partially or fully removed. It also complements existing research on Bohai coastal restoration [10,27] by linking local morphological features to system-scale stability. Therefore, the fundamental contribution of this study lies in proposing

that tidal-flat restoration in semi-enclosed bays should be evaluated not only in terms of reclaimed area removed, but also in terms of how the inherited tidal creek network modulates hydrodynamic adjustment and sediment response.

4.6.3. Advantages of Combined Removal–Dredging Restoration

Full reclamation removal alone increases the tidal prism only marginally, whereas supplementary tidal creek dredging further improves the bay's water exchange efficiency by expanding the tidal conveyance channel. Therefore, the combined scheme balances ecological safety and restoration benefits, making it suitable for application in similar northern semi-enclosed estuarine bays.

4.6.4. Research Limitations

This simulation ignores seasonal river runoff input, sea-ice effects (a typical feature of high-latitude Liaodong Bay [21]), and long-term wind–wave-induced sediment resuspension; future research can incorporate ice–wave–current coupling to refine the prediction of long-term morphological evolution.

Furthermore, the present two-dimensional depth-averaged model inherently cannot capture vertical stratification effects and vertical sediment concentration gradients, which may influence erosion and deposition processes in deeper channels. The assumption of depth-averaged flow is justified for this study area where the water depth is relatively uniform (mostly <5 m) and tidal mixing is strong, minimizing vertical density gradients. However, for future studies in deeper or more stratified environments, a three-dimensional model extension would be advisable. Additionally, the sediment transport formulation in the current model employs a simplified approach; incorporating detailed bed load transport formulas (e.g., Meyer-Peter and Muller formula), settling velocity assumptions based on grain size distribution, and critical erosion threshold parameters specific to the study area sediments would further improve the predictive capability of the model.

Based on the limitations identified in this study, future research should: (1) incorporate seasonal river runoff input and its sediment supply to assess how fluvial processes interact with tidal dynamics during restoration; (2) extend the numerical model to three dimensions to capture vertical stratification and sediment concentration gradients in deeper channels; (3) incorporate long-term wind–wave forcing and sea-ice effects to improve predictions of morphological evolution under climate change scenarios; (4) conduct field monitoring campaigns post-restoration to validate model predictions and refine parameter calibration; and (5) integrate economic cost–benefit analysis and engineering feasibility assessment to support decision-making for large-scale restoration projects. These improvements would enhance the robustness of numerical tools for coastal restoration planning in temperate semi-enclosed bays.

5. Conclusions and Outlook

Based on the numerical model simulations in this study, the following conclusions are drawn:

(1) In the northern waters of Liaodong Bay, reclamation removal induces spatially limited hydrodynamic modifications that are confined to within 500 m of the project area, without altering the large-scale tidal circulation of Liaodong Bay and the Liaohe Estuary. The natural tidal creek system plays a dominant buffering role in suppressing far-field environmental disturbance.

(2) The spatial distribution patterns of suspended sediment remain stable under all restoration schemes; only S4 reduces the local peak suspended-sediment concentration through

enhanced tidal flushing. Regional seabed erosion–deposition undergoes only mild changes, and S4 is more conducive to restoring the natural nearshore geomorphology.

(3) The tidal prism increases with restoration intensity: +0.51% for partial removal, +1.27% for full removal, and +2.17% for full removal combined with tidal creek dredging. This increase is more pronounced during spring tides. Although these absolute increases are modest, they are practically meaningful from a restoration perspective. In semi-enclosed estuarine bays with extensive intertidal flats, even small increases in tidal prism can enhance tidal flushing, improve water exchange within the tidal creek network, and promote more frequent inundation and drainage of restored tidal flats. This mechanism is consistent with previous findings that tidal creek dredging and reclamation removal can restore hydrological connectivity and improve local ecological conditions [1,8,19]. Therefore, the reported increases should not be interpreted as basin-scale hydraulic transformations, but as ecologically relevant improvements in local tidal exchange capacity.

(4) Reclamation removal that avoids main tidal creek channels is a low-disturbance, eco-friendly restoration measure; the composite mode of full demolition plus tidal creek dredging emerges as the most favorable restoration approach among the scenarios tested in this study for semi-enclosed estuarine bays in northern China.

(5) Several limitations should be addressed in future work. First, the present model does not explicitly include sediment input from river runoff. Because the Liaohe Estuary supplies fine-grained sediment to adjacent tidal flats, river-derived sediment may locally enhance deposition in nearshore and creek-mouth areas, especially during flood seasons [3,6,9,20]. Second, sediment supply from river runoff may interact with the enhanced tidal flushing produced by reclamation removal and tidal creek dredging. Under higher sediment supply, increased tidal exchange could transport more suspended sediment into restored areas, potentially accelerating vertical accretion of tidal flats; under lower sediment supply, the same hydrodynamic enhancement may favor sediment export and mild bed erosion. Third, future studies should couple seasonal river runoff, wave forcing, and vegetation recovery with the present hydrodynamic–sediment model, so that the long-term morphodynamic evolution and ecological effectiveness of different restoration schemes can be assessed more comprehensively. In particular, the model should be extended from the current two-dimensional depth-averaged framework to a three-dimensional formulation to better resolve vertical structure in tidal currents, sediment stratification, and density-driven circulation associated with seasonal freshwater input. Given the regional setting of northern Liaodong Bay, wind–wave effects and sea-ice processes should also be incorporated, because wave-induced bed shear stress can significantly modify nearshore sediment resuspension and transport, while seasonal sea ice may alter tidal exchange, dampen wave energy, and influence winter morphodynamics and habitat conditions. In parallel with numerical development, post-restoration field monitoring should be conducted to validate model predictions and to track changes in bathymetry, suspended-sediment concentration, tidal creek morphology, water quality, and benthic or vegetation communities. Finally, restoration assessment should be complemented by an economic cost–benefit analysis that compares engineering expenditure, maintenance requirements, ecological gains, fisheries and habitat benefits, and long-term risk reduction, thereby providing a more practical basis for selecting restoration strategies in semi-enclosed estuarine bays.

Author Contributions: Conceptualization, K.W., L.S., N.L. and J.W.; methodology, K.W.; software, C.H.; validation, K.W.; verification, L.S.; investigation, G.S., C.H. and Z.W.; writing—initial draft preparation, K.W.; writing—review and editing, N.L. and Y.G.; visualization, C.H.; supervision, L.S.; funding acquisition, L.S. All authors have read and agreed to the published version of the manuscript.

Funding: This work was supported by the Fundamental Research Funds of Liaoning Academy of Agricultural Sciences (Grant No. 2025XKJS8578) and the Sci-Tech Innovation Special Program of the Liaoning Academy of Agricultural Sciences (Grant No. 2026CY3535).

Data Availability Statement: The original contributions presented in this study are included in the article. Further inquiries can be directed to the corresponding authors.

Conflicts of Interest: The authors declare no conflicts of interest.

References

1. Jia, R.; Lei, H.; Hino, T.; Arulrajah, A. Environmental changes in Ariake Sea of Japan and their relationships with Isahaya Bay reclamation. *Mar. Pollut. Bull.* **2018**, *135*, 832–844. [CrossRef]
2. Gao, G.D.; Wang, X.H.; Bao, X.W.; Song, D.; Lin, X.P.; Qiao, L.L. The impacts of land reclamation on suspended-sediment dynamics in Jiaozhou Bay, Qingdao, China. *Estuar. Coast. Shelf Sci.* **2018**, *206*, 61–75. [CrossRef]
3. Zhang, G.; Chen, Y.; Cheng, W.; Zhang, H.; Gong, W. Wave effects on sediment transport and entrapment in a channel-shoal estuary: The Pearl River Estuary in the dry winter season. *J. Geophys. Res. Oceans* **2021**, *126*, e2020JC016905. [CrossRef]
4. Zhang, W.L.; Guo, J.L.; Liu, Z.C.; Shi, L.Q.; Gong, Z.H.; Zhang, D.H. Analysis of spatial and temporal shoreline changes and reclamation in the Qinzhou Bay and the Manila Bay. *Trop. Geogr.* **2025**, *45*, 489–503. (In Chinese) [CrossRef]
5. Li, W.D.; Zhu, Z.Y.; Chen, N.W.; Xu, T.; Sun, Z.X. Impacts of coastal reclamation projects on tidal prism in the Jiulong River Estuary. *J. Waterw. Harb.* **2024**, *45*, 495–501.
6. Han, H.H.; Gao, F.; Ding, D.; Ma, L. Influence of reclamation project on tidal volume and water exchange in Sanmen Bay. *Mar. Geol. Front.* **2024**, *40*, 40–50. [CrossRef]
7. Dong, H. Numerical Simulation of the Impact of Approach Bridge Facilities on Flow Field in a Sea Area of the South China Sea. Master's Thesis, Dalian University of Technology, Dalian, China, 2023.
8. Wang, L.Q. Study on Water-Sediment Movement and Evolution Characteristics of the Liaohe River Estuary. Master's Thesis, Hohai University, Nanjing, China, 2005.
9. Wang, D.M.; Wang, X.D.; Chen, J.; Li, X.; Zhu, H.Y. Analysis of suspended sediment transport characteristics in the Liaohe River Estuary. *Sci. Technol. Inf.* **2008**, 71–72. [CrossRef]
10. Hou, X.Y.; Zhang, H.; Li, D.; Hou, W.; Song, Y. Development trend, environmental and ecological impacts, and policy recommendations for Bohai Sea reclamation. *Acta Ecol. Sin.* **2018**, *38*, 3311–3319. [CrossRef]
11. Wang, R. Study on Hydrodynamic Environmental Impacts of Coastal Reclamation in the Bohai Sea Based on FVCOM. Master's Thesis, Tianjin University, Tianjin, China, 2018.
12. Wang, P.; Zou, W.F.; Dong, X.K.; Sun, J.W.; Zhang, N.C. Analysis of the influence of tidal creek dredging on tidal flat hydrodynamics. *Coast. Eng.* **2023**, *42*, 174–187. [CrossRef]
13. Palacios, M.M.; Martin, R.; Wartman, M.; Rowland, P.I.; Macreadie, P.I.; Ross, F.W.R.; Young, A.R.; Costa, M.D.P. Tidal reinstatement of coastal wetlands: A global review. *Restor. Ecol.* **2026**, *34*, e70347. [CrossRef]
14. Slinger, J.; Stive, M.; Luijendijk, A. Nature-based solutions for coastal engineering and management. *Water* **2021**, *13*, 976. [CrossRef]
15. Kiesel, J.; MacPherson, L.R.; Schuerch, M.; Vafeidis, A.T. Can managed realignment buffer extreme surges? The relationship between marsh width, vegetation cover and surge attenuation. *Estuaries Coasts* **2022**, *45*, 345–362. [CrossRef]
16. Türker, U.; Yagci, O.; Kabdasli, M.S. Impact of nearshore vegetation on coastal dune erosion: Assessment through laboratory experiments. *Environ. Earth Sci.* **2019**, *78*, 584. [CrossRef]
17. Petti, M.; Pascolo, S.; Bosa, S.; Busetto, N. On the tidal prism: The roles of basin extension, bottom friction and inlet cross-section. *J. Mar. Sci. Eng.* **2021**, *9*, 88. [CrossRef]
18. Kuang, C.; Li, H.; Huang, G.; Han, X.; Zou, Q.; Song, H. Sediment transport and morphological responses of a silty coast to a cold front event in the southwest Bohai Bay of China. *Estuar. Coast. Shelf Sci.* **2022**, *278*, 108106. [CrossRef]
19. Yuan, Y.; Jalón-Rojas, I.; Wang, X.H. Response of water-exchange capacity to human interventions in Jiaozhou Bay, China. *Estuar. Coast. Shelf Sci.* **2021**, *249*, 107088. [CrossRef]
20. Ji, C. Numerical Simulation of Three-Dimensional Sediment Transport and Beach Evolution Under Wave-Current Coupling. Ph.D. Thesis, Tianjin University, Tianjin, China, 2019.
21. Zhang, N.; Wang, J.; Wu, Y.; Wang, K.-H.; Zhang, Q.; Wu, S.; You, Z.-J.; Ma, Y. A modelling study of ice effect on tidal damping in the Bohai Sea. *Ocean Eng.* **2019**, *173*, 748–760. [CrossRef]
22. Chen, B. Numerical Simulation of Three-Dimensional Suspended Sediment in Waters Adjacent to the Yangtze River Estuary. Ph.D. Thesis, Graduate University of Chinese Academy of Sciences (Institute of Oceanology), Beijing, China, 2008.
23. Wen, H.Y. Numerical Simulation of Coastal Sediment Transport and Its Application. Master's Thesis, Dalian University of Technology, Dalian, China, 2008.

24. Cao, X.F.; Zhang, Y.M.; Zhang, S.F.; Shi, W.Q.; Li, Q.J.; Shi, H.Y.; Wang, P.; Wang, Y.; Zhao, Q.; Han, C.W. Study on water exchange capacity of Dalian Bay based on numerical simulation. *Mar. Environ. Sci.* **2020**, *39*, 114–120. [CrossRef]
25. Nie, C.H.; Wu, Y.Y.; Zhu, J.L.; Xu, Y.D.; Du, P.; Wang, H. Numerical study on hydrodynamic effects of coastline changes in southwestern Laizhou Bay. *Mar. Environ. Sci.* **2023**, *42*, 228–236. [CrossRef]
26. Wang, K.; Li, N.; Song, G.J.; Guan, C.J.; Hu, C.K.; Du, J.; Shao, Z.W.; Wu, J.H. Ecological dynamics model of phytoplankton distribution in Liaodong Bay. *J. Dalian Ocean Univ.* **2022**, *37*, 1004–1012. (In Chinese) [CrossRef]
27. Liu, M.; Xi, X.H.; Lei, L.Y.; Zhang, X.; Bi, Y.P. The effects of coastal reclamation on hydrodynamics in Jinzhou Bay. *J. Dalian Ocean Univ.* **2013**, *28*, 110–114.
28. Fan, X.H. Habitat Construction and Ecological Effects of Typical Plants for Northern Ecological Seawalls. Master's Thesis, Dalian University of Technology, Dalian, China, 2023.
29. Liu, Y.P.; Zhang, Z. Evolution characteristics of water and sediment in the Liaohe River Estuary. *Northeast. Water Resour. Hydropower* **2005**, *23*, 38–40. [CrossRef]
30. Wang, K.; Li, N.; Wang, Z.; Song, G.; Du, J.; Song, L.; Jiang, H.; Wu, J. The impact of floating raft aquaculture on the hydrodynamic environment of an open sea area in Liaoning Province, China. *Water* **2022**, *14*, 3125. [CrossRef]
31. Smagorinsky, J. General circulation experiments with the primitive equations: I. Basic Experiment. *Mon. Weather Rev.* **1963**, *91*, 99–164. [CrossRef]
32. Wang, K.; Li, N.; Song, L.; Wu, J.; Jiang, H. Application of a VOF multiphase flow model for issues concerning floating raft aquaculture. *Water* **2023**, *15*, 3450. [CrossRef]
33. Guan, C.J.; Wang, K.; Tian, X.H.; Xu, P.; Lu, H.L.; Liu, Y.J.; Zhao, X.X.; Kong, F. Numerical simulation of drift paths of drifting algae in waters near nuclear power plants. *J. Appl. Oceanogr.* **2022**, *41*, 229–239. (In Chinese) [CrossRef]
34. Zhao, X.D.; Sun, J.W.; Sun, Z.C.; Liang, S.X. Wet-dry boundary treatment technology based on CC-CV hybrid finite volume method and its application in shallow water problems. *J. Waterw. Harb.* **2017**, *38*, 548–554.
35. Lu, Y.J. Three-Dimensional Turbulent Flow-Sediment Numerical Model and Its Application. Ph.D. Thesis, Nanjing Hydraulic Research Institute, Nanjing, China, 2002.

Disclaimer/Publisher's Note: The statements, opinions and data contained in all publications are solely those of the individual author(s) and contributor(s) and not of MDPI and/or the editor(s). MDPI and/or the editor(s) disclaim responsibility for any injury to people or property resulting from any ideas, methods, instructions or products referred to in the content.